Abdlmanam S. A. Elmaryami[1], Amal A. E. Mohamed[2]*

[1]The Bright Star University [BSU], El-Brega, Libya,
[2]University of Tobruk,Tobruk, Libya

Scientificpaper
ISSN 0351-9465, E-ISSN 2466-2585
https://doi.org/10.5937/zasmat2303327E

Zastita Materijala 64 (3)
327 - 339 (2023)

A Novel 2-D mathematical modeling to determine LHP to protectthe industrial transient heat treatment quenched low carbon steels bar

ABSTRACT

2-dimensional mathematical model of axisymmetric transient industrial quenched low carbon steel bar, to examine the influence of process history on metallurgical and material characteristics, a water-cooled model based on the finite element technique was adopted. A 2-dimensional axisymmetric mathematical model was utilized to predict temperature history and, as a result, the hardness of the quenched steel bar at any node (point). The LHP (lowest hardness point) is evaluated. In this paper, specimen points hardness was evaluated by the transformation of determined characteristic cooling time for phase conversion $t_{8/5}$ to hardness. The model can be used as a guideline to design cooling approach to attain the desired microstructure and mechanical properties, for example, hardness. The mathematical model was verified and validated by comparing its hardness results to the results of commercial finite element software. The comparison demonstrates that the proposed model is reliable.

Keywords: *Heat treatment; quenching; axisymmetric steel bar; finite element; 2-D mathematical modelling ;unsteady state heat transfer.*

1. INTRODUCTION

Quenching is a type of heat treatment that is commonly used in industrial processes to control mechanical properties of steels such as hardness [1]. Galerkin free element method – GFrEM combines the advantages of the finite element method and meshfree method in the aspects of setting up shape functions and generating computational meshes through node by node [2]. The procedure entails raising the steel temperature above a critical value, keeping it at that temperature for a specified time, and then rapidly cooling it to room temperature in a suitable medium [3]**.** Galerkin's method of weighted residual was applied to study the heat transfer and thermal stability of a convective straight fin with temperature-dependent thermal conductivity and internal heat generation [4].

The microstructures formed during quenching (ferrite, cementite, pearlite, upper bainite, lower bainite, and martensite) are affected by the cooling rate as well as the chemical composition of the steel [5].

The investigation is concerned with the development of non-power series solutions for the unsteady state nonlinear thermal model of a radiative-convective fin having temperature-variant thermal conductivity using Laplace transform-Galerkin weighted residual method [6].

Steel quenching is a multi-physics process that involves a complex pattern of heat transfer couplings. Because of the complexity, there is no analytical solution exists of coupled (thermal-mechanical-metallurgical) theory and non-linear nature of the problem.However, numerical solutions can be obtained using the finite difference method, the finite volume method, and the most widely used method - the finite element method (FEM) [**7**].

Heat transfer is a critical function in many technical, industrial, home, and commercial structures. As a result, the purpose of this study is to investigate the effects of slip velocity and variable fluid characteristics on Cassonbionanofluid flow across a stretching sheet that has been saturated by gyrotactic microorganisms. The suggested system will be converted to a computationally tractable form using the Galerkin method [8].

*Corresponding autor: Abdlmanam S. A. Elmaryami
E-mail: damer604@yahoo.com
Paper received: 20. 03. 2023.
Paper corrected: 11.05.2023.
Paper accepted: 15. 05. 2023.
Paperisavailableonthewebsite:www.idk.org.rs/journal

The heat transfer is unsteady during the quenching process of the steel bar because temperature varies with time [**9**]. A new numerical approach to solving the fractional differential Riccati equations numerically. The approach—called the Mittag-Leffler–Galerkin method—comprises the finite Mittag-Leffler function and the Galerkin method [10].

In order to obtain the numerical results of 3D convection-diffusion-reaction problems with variable coefficients efficiently, The improved element-free Galerkin (IEFG) method instead elected of the traditional element-free Galerkin (EFG) method by using the improved moving leastsquares (MLS) approximation to obtain the shape function [11].

A lot of essential consciences substantial and synthetic experience can be described by Partial Differential Equation (PDE). These Galerkin method (GM) and Collocation method (CM) are used to solve some examples of nonlinear Partial Differential Equation (PDE). The particular times is used in these methods because it can influence the collected result from the solution to be compared in terms of convergence study and the accuracy of the numerical solution [12].

The work explores an error analysis of Galerkin finite element method (GFEM) for computing steady heat conduction in order to show its convergence and accuracy. The steady state heat distribution in a planar region is modeled by two-dimensional Laplace partial differential equations. A simple three-node triangular finite element model is used and its derivation to form elemental stiffness matrix for unstructured and structured grid meshes is presented [13].

The aim has been to deal with numerical solution of two dimensional hyperbolic boundary value problem. By applying Galerkin method for solution of this problem, numerical results are obtained and these results are compared with analytical solutions [14].

Numerical solutions obtained by the meshless local Petrov-Galerkin (MLPG) method are presented for 2-D functionally graded solids, which is subjected to either mechanical or thermal loads. The MLPG method is a truly meshless approach, as it does not need any background mesh for integration in the weak form.

In this MLPG analysis, the penalty method is used to efficientlyenforce the essential boundary conditions, and the test function is chosen to equal the weight function of the moving least squares approximation [15].

A novel weak-form block Petrov–Galerkin method (BPGM) for linear elastic and crack problems in functionally graded materials with bounded and unbounded problem domains. The main idea of this approach is to combine the meshless local Petrov–Galerkin method with block method. Once the problem domain is discretized into several sub-regions, named blocks, which can be mapped into normalized square domains. The weak-form Petrov–Galerkin method and polynomial series of interpolations are employed in each block. The computational efficiency is rigorously examined against the strong-form finite block method, the finite element technique and meshless approaches [16].

The improved element-free Galerkin (IEFG) method is proposed for solving 3D Helmholtz equations. The improved moving least-squares (IMLS) approximation is used to establish the trial function, and the penalty technique is used to enforce the essential boundary conditions. Thus, the final discretized equations of the IEFG method for 3D Helmholtz equations can be derived by using the corresponding Galerkin weak form. The influences of the node distribution, the weight functions, the scale parameters of the influence domain, and the penalty factors on the computational accuracy of the solutions are analyzed [17].

The heat transfer analysis in this paper will be conducted in three dimensions. To reduce cost and computer time, the three-dimensional analysis will be simplified to a two-dimensional axisymmetric analysis [7,18-22]. This is achievable because in axisymmetric conditions, the temperature deviations is only in (R) and (Ɵ) while there is no temperature variation in the (z) direction as seen on Figure1.

The Galerkin weighted residual technique is utilized to prove the mathematical approach [23-28]. In this research 2-dimensional will be adopted to determine LHP.

2. MATHEMATICAL APPROACH

The temperature history of the quenched cylindrical steel bar should be evaluated at any point; three-dimensional heat transfer can be examined using two-dimensional axisymmetricelements, as illustrated in Figure 1.

Temperature distribution approximation for an arbitrary linear triangular element [Saeed Moavani, 1999]:

$$T^{(e)} = a_1 + a_2 R + a_3 Z \qquad (1)$$

R and Z is any point inside the element itself, based on global body.

The area for triangular element [Ismail Sharif 2005]:

$$A = \frac{1}{2} det \begin{vmatrix} 1 & R_i & Z_i \\ 1 & R_j & Z_j \\ 1 & R_k & Z_k \end{vmatrix}$$

$$\left(R_j Z_k - R_j Z_i + R_k Z_i - R_k Z_j + R_i Z_j - R_i Z_k\right) = 2A \qquad (2)$$

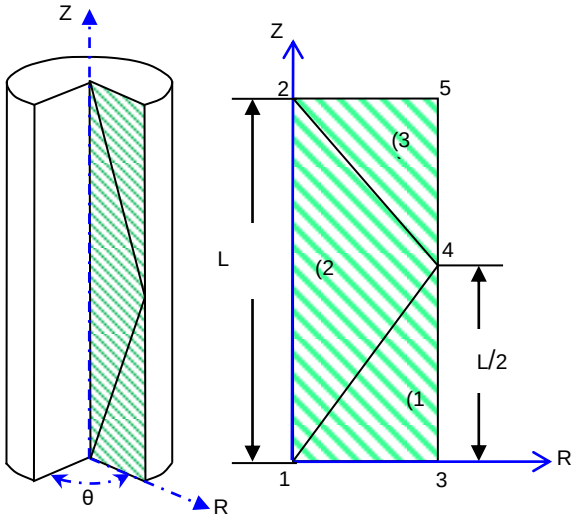

Figure 1. This image clearly represented axisymmetric element from the domain

Slika 1.Predstavljen je osnosimetričan element iz domena

Shape function of 2-Dimentional Axi-symmetric triangularelement.

The field variable's variation over the element was to be represented by the shape functions. The shape function of the axi-symmetric triangular element are expressed in terms of the r and z coordinates typically used for axi-symmetric triangular elements and its coordinates as seen in Figur 2.

Which are proved to produce the shape functions that are demonstrated below;

$$S_i = \left(\frac{1}{2A}\right)\left(\alpha_i + \beta_i r + \delta_i z\right) \qquad (3)$$

$$S_j = \left(\frac{1}{2A}\right)\left(\alpha_j + \beta_j r + \delta_j z\right) \qquad (4)$$

$$S_k = \left(\frac{1}{2A}\right)\left(\alpha_k + \beta_k r + \delta_k z\right) \qquad (5)$$

Where;

$$\alpha_i = R_j Z_k - R_k Z_j ; \beta_i = Z_j - Z_k ; \delta_i = R_K - R_j$$

$$\alpha_j = R_k Z_i - R_i Z_k ; \beta_j = Z_k - Z_i ; \delta_j = R_i - R_k$$

$$\alpha_k = R_i Z_j - R_j Z_i ; \beta_k = Z_i - Z_j ; \delta_k = R_j - R_i$$

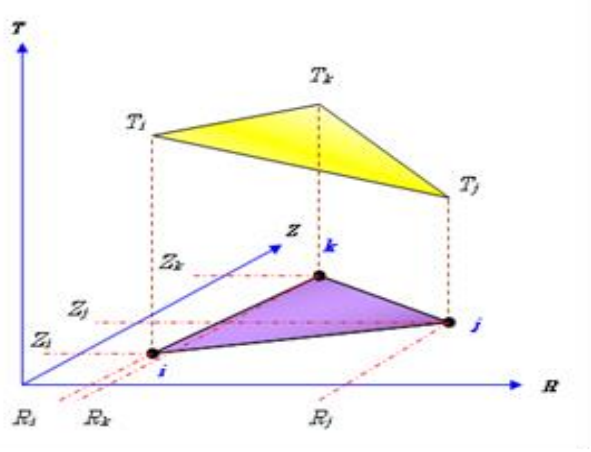

Figure 2. The global coordinate system of a typicaltriangular elements

Slika 2.Globalni koordinatni sistem tipičnih trouglastih elemenata

Natural area coordinate

For a triangular element, the natural area coordinates; ξ, η, λ are defined as shown in Figure 3. by:

$$\xi = \frac{A_1}{A}, \eta = \frac{A_2}{A}, \lambda = \frac{A_3}{A} \qquad (6)$$

The triangular natural area coordinates are exactly identical to the shape functions S_i, S_j, S_k

$$\xi = S_i,\ \eta = S_j,\ \lambda = S_k \qquad (7)$$

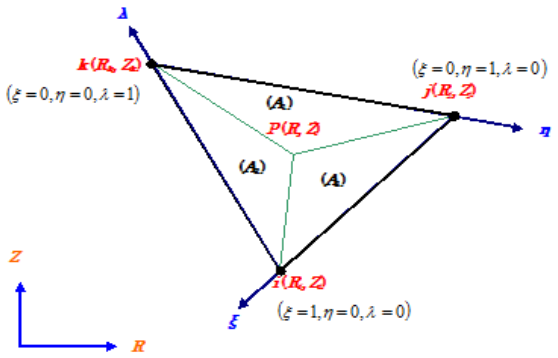

Figure 3. Natural coordinates used for a triangularelement

Slika 3.Prirodne koordinate koje se koriste za trouglasti element

Derivation of the heat conduction equation in Axi-symmetric elements

Figure 4 illustrates the application of energy conservation to a differential volume cylindrical section

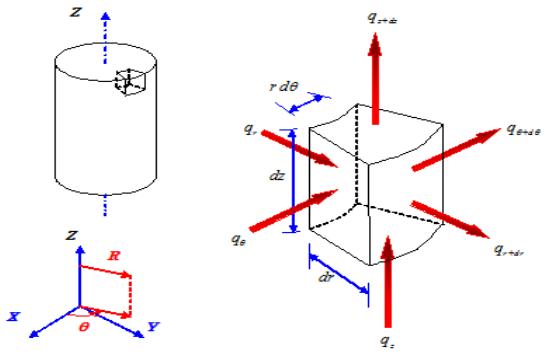

Figure 4. Axi-symetric element from an Axisymetric body

Slika 4.Osnosimetrični element iz Aki simetričnog tela

$$E_{in} - E_{out} + E_{generated} = E_{stored} \quad (8)$$

By reducing the differential volume term, the heat transfer-transient through the component during quenching can be mathematically represented; the heat conduction equation is proved and provided by; Eq. 9.

$$\frac{1}{r}\frac{d}{dr}\left(K_r r\frac{dT}{dr}\right)+\frac{1}{r^2}\frac{d}{d\theta}\left(K_\theta\frac{dT}{d\theta}\right)+\frac{d}{dz}\left(K_z\frac{dT}{dz}\right)+q=\rho c\frac{dT}{dt} \quad (9)$$

k_z = coefficient of heat conductivity in *z*-direction, W/m·°C

k_r = coefficient of heat conductivity in *r*-direction, W/m·°C

k_θ = coefficient of heat conductivity in *θ*-direction, W/m·°C

t =time, s

c = medium's specific heat, J/kg·K

q = heat generation, W/m^3

T = temperature, °C

ρ = mass density, kg/m^3

Formulation of the Galerkin Weighted Residual Method

From the obtained equation of heat conduction, the Galerkin residual for the triangular element in an unsteady state heat transfer by integration the shape functions times the residual that reduces the residual to zero;

$$[R]^{(e)}=\int_v[S]^T\left(\frac{k}{r}\frac{d}{dr}\left(r\frac{dT}{dr}\right)+k\frac{d^2T}{dz^2}+q\right)dv-$$
$$-\int_v[S]^T\left(\rho c\frac{dT}{dt}\right)dv=0 \quad (10)$$

$$\int_V[S]^T\{\Re\}^{(e)}dV=2\pi\iint_A[S]^T\{\Re\}\bar{r}drdz \quad (11)$$

Thus Eq. 10 consists of four parts as shown in Eq. 12;

$$=2\pi k\iint_A[S]^T\left\{\frac{\partial}{\partial r}\left(\bar{r}\frac{\partial T}{\partial r}\right)\right\}drdz+2\pi k\iint_A[S]^T\left\{\frac{\partial}{\partial z}\left(\bar{r}\frac{\partial T}{\partial z}\right)\right\}drdz$$
$$+2\pi\iint_A[S]^T\dot{q}\bar{r}drdz-2\pi\iint_A[S]^T\left\{\rho c\,\bar{r}\frac{\partial T}{\partial t}\right\}drdz \quad (12)$$

where:

$$[S]^T=\begin{Bmatrix}S_i\\S_j\\S_k\end{Bmatrix}$$

values of shape functions are as shown in equation 3, 4 and 5.

Chain rule

The Term 1 and 2 of Eq. 12 can be re-arranged using the chain rule which states that;

$$(fg)^-=fg^-+gf^- \quad (13)$$

Therefore, $fg^-=(fg)^--f^-g$

Term 1 of Eq. 12 is rearranged thus;

$$[S]^T\left\{\frac{\partial}{\partial r}\left(\bar{r}\frac{\partial T}{\partial r}\right)\right\}=\frac{\partial}{\partial r}\left([S]^T\bar{r}\frac{\partial T}{\partial r}\right)-\frac{\partial[S]^T}{\partial r}\bar{r}\frac{\partial T}{\partial r} \quad (14)$$

Similarly, Term 2 of Eq. 12 is rearranged thus;

$$[S]^T\left(\frac{\partial^2T}{\partial z^2}\right)=\frac{\partial}{\partial z}\left([S]^T\bar{r}\frac{\partial T}{\partial z}\right)-\frac{\partial[S]^T}{\partial z}\bar{r}\frac{\partial T}{\partial z} \quad (15)$$

Thus Eq. (12) becomes consists of six parts as shown in Eq.16;

$$=\overbrace{2\pi k\iint_A\left\{\frac{\partial}{\partial r}\left([S]^T\bar{r}\frac{\partial T}{\partial r}\right)\right\}drdz}^{A}-\overbrace{2\pi k\iint_A\left\{\frac{\partial[S]^T}{\partial r}\bar{r}\frac{\partial T}{\partial r}\right\}drdz}^{B}+$$
$$\overbrace{2\pi k\iint_A\left\{\frac{\partial}{\partial z}\left([S]^T\bar{r}\frac{\partial T}{\partial z}\right)\right\}drdz}^{C}-\underbrace{2\pi k\iint_A\left\{\frac{\partial[S]^T}{\partial z}\bar{r}\frac{\partial T}{\partial z}\right\}drdz}_{D}+$$
$$\underbrace{2\pi\iint_A[S]^T\dot{q}\bar{r}drdz}_{E}-\underbrace{2\pi\iint_A[S]^T\left\{\rho c\bar{r}\frac{\partial T}{\partial t}\right\}drdz}_{F} \quad (16)$$

Note that Eq. 14 and 15 each consists of two Terms, the first Terms (A and C) in Eq. 16 are the heat convection terms and the second Terms of each of the Eqs. (B and D) in Eq. 16 are the heat conduction terms. Considering Eqs. (B and D) which are the heat conduction terms, both terms are evaluated to obtain the conductance matrices

in the r and z direction respectively, therefore we have that; for Eq. B,

$$\frac{\partial[S]^T}{\partial r}=\frac{\partial}{\partial r}\begin{Bmatrix}S_i\\S_j\\S_k\end{Bmatrix}=\frac{\partial}{\partial r}\begin{Bmatrix}\frac{1}{2A}(\alpha_i+\beta_i R+\delta_i Z)\\\frac{1}{2A}(\alpha_j+\beta_j R+\delta_j Z)\\\frac{1}{2A}(\alpha_k+\beta_k R+\delta_k Z)\end{Bmatrix}=\frac{1}{2A}\begin{Bmatrix}\beta_i\\\beta_j\\\beta_k\end{Bmatrix} \quad (17)$$

where:

$$\frac{\partial T}{\partial r}=\frac{\partial}{\partial r}\begin{bmatrix}S_i & S_j & S_k\end{bmatrix}\begin{Bmatrix}T_i\\T_j\\T_k\end{Bmatrix} \quad (18)$$

$$\bar{r}=S_iR_i+S_jR_j+S_kR_k=\frac{R_i+R_j+R_k}{3} \quad (19)$$

[Stasa, F. L. (1985) Pappus-Guldinus theorem]

After Substituting Eq. 17, 18 and 19 in Eq. B and simplifying, we get

$$=\frac{\pi k\left(R_i+R_j+R_k\right)}{6A}\begin{bmatrix}\beta_i^2 & \beta_i\beta_j & \beta_i\beta_k\\\beta_i\beta_j & \beta_j^2 & \beta_j\beta_k\\\beta_i\beta_k & \beta_j\beta_k & \beta_k^2\end{bmatrix}\begin{Bmatrix}T_i\\T_j\\T_k\end{Bmatrix} \quad (20)$$

Similarly, Eq. D in z-direction,

$$=\frac{\pi k\left(R_i+R_j+R_k\right)}{6A}\begin{bmatrix}\delta_i^2 & \delta_i\delta_j & \delta_i\delta_k\\\delta_i\delta_j & \delta_j^2 & \delta_j\delta_k\\\delta_i\delta_k & \delta_j\delta_k & \delta_k^2\end{bmatrix}\begin{Bmatrix}T_i\\T_j\\T_k\end{Bmatrix} \quad (21)$$

Note in our case quenching from austenitization temperature to the ambient temperature thus no heat generation within the element, it means no the thermal load due to heat generation, therefore Eq. E become zero;

Thus Eq.

$$E=\iint_A[S]^T\,\dot{q}\,\bar{r}\,drdz=2\pi\,\dot{q}\iint_A[S]^T\,\bar{r}\,drdz \quad (22)$$

Green's theorem

The Green's theorem is used to re-write area integrals in terms of line integral around the element boundary[**29-35**]. This theorem is applied to Eq. A and Eq. C.

$$2\pi k\iint_A\left\{\frac{\partial}{\partial r}\left([S]^T\bar{r}\frac{\partial T}{\partial r}\right)\right\}drdz=2\pi k\int_\tau[S]^T\bar{r}\frac{\partial T}{\partial r}\cos\theta\,d\tau \quad (23)$$

$$2\pi k\iint_A\left\{\frac{\partial}{\partial z}\left([S]^T\bar{r}\frac{\partial T}{\partial z}\right)\right\}drdz=2\pi k\int_\tau[S]^T\bar{r}\frac{\partial T}{\partial z}\sin\theta\,d\tau \quad (24)$$

The combination of Eq. 23 and 24;

$$=2\pi k\int_\tau[S]^T\bar{r}\frac{\partial T}{\partial r}\cos\theta\,d\tau+2\pi k\int_\tau[S]^T\bar{r}\frac{\partial T}{\partial z}\sin\theta\,d\tau \quad (25)$$

After substituting in Eq. 25 and simplifying, where the conservation of energy is applied on the r- and z-direction

$$q''_{conduction}=q''_{convection}=-k\frac{\partial T}{\partial r}=h(T-T_f)=-k\frac{\partial T}{\partial z}\text{, we get;}$$

$$=-2\pi\bar{r}h\int_\tau[S]^T(T)d\tau+2\pi rh\int_\tau[S]^T(T_f)d\tau \quad (26$$

If there is a possible convection on the elements edge Fig. 5 and Fig. 6, the first Terms of Eq. 26 contributes to the conductance matrix as shown;)

Along i - j,

$$\frac{\partial T}{\partial t}=\frac{\partial}{\partial t}([S]\{T\})$$

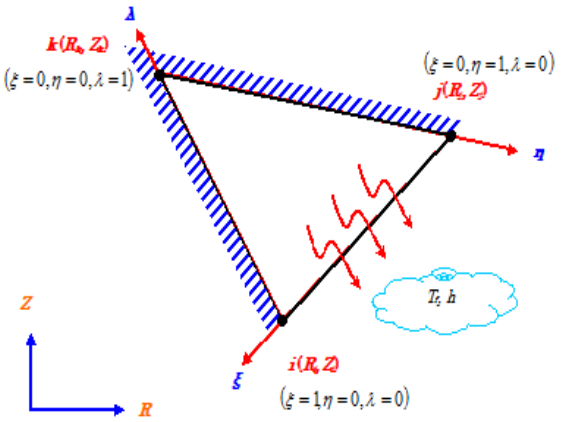

Figure 5. Possible convection through ij-edge

Slika 5. Moguća konvekcija kroz ij-ivicu

$$[K]^{(e)}=\frac{2\pi hl_{ij}}{12}\begin{bmatrix}3R_i+R_j & R_i+R_j & 0\\R_i+R_j & R_i+3R_j & 0\\0 & 0 & 0\end{bmatrix} \quad (27)$$

Along j - k,

$$2\pi\iint_A[S]^T\left\{\rho\,c\,\bar{r}\frac{\partial T}{\partial t}\right\}drdz$$

$$=\frac{2\pi\rho\,cA}{60}\begin{bmatrix}\left(6R_i+2R_j+2R_k\right) & \left(2R_i+2R_j+R_k\right) & \left(2R_i+R_j+2R_k\right)\\\left(2R_i+2R_j+R_k\right) & \left(2R_i+6R_j+2R_k\right) & \left(R_i+2R_j+2R_k\right)\\\left(2R_i+R_j+2R_k\right) & \left(R_i+2R_j+2R_k\right) & \left(2R_i+2R_j+6R_k\right)\end{bmatrix}\begin{Bmatrix}\dot{T}_i\\\dot{T}_j\\\dot{T}_k\end{Bmatrix}$$

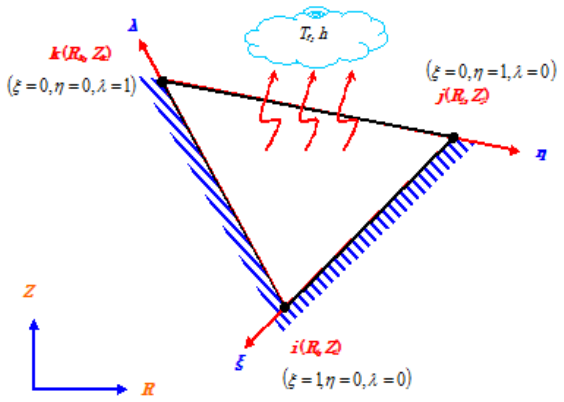

Figure 6. Possible convection through jk-edge

Slika 6. Moguća konvekcija kroz jk-ivicu

$$[K]^{(e)} = \frac{2\pi h l_{jk}}{12}\begin{bmatrix} 0 & 0 & 0 \\ 0 & 3R_j + R_K & R_j + R_k \\ 0 & R_j + R_k & R_j + 3R_K \end{bmatrix} \quad (28)$$

Along k - i,

$$[K]^{(e)} = \frac{2\pi h l_{ki}}{12}\begin{bmatrix} 3R_i + R_k & 0 & R_i + R_k \\ 0 & 0 & 0 \\ R_i + R_k & 0 & R_i + 3R_K \end{bmatrix} \quad (29)$$

If there is a possible convection at the element edge, the second terms of Eq. 26 contribute to the thermal load matrix as shown;

Along i – j

$$[F]^{(e)} = \frac{2\pi h T_f l_{ij}}{6}\begin{bmatrix} 2R + R_j \\ R_i + 2R_j \\ 0 \end{bmatrix} \quad (30)$$

Along

$$j-k, [F]^{(e)} = \frac{2\pi h T_f l_{jk}}{6}\begin{bmatrix} 0 \\ 2R_j + R_k \\ R_j + 2R_k \end{bmatrix} \quad (31)$$

Along

$$k-i, [F]^{(e)} = \frac{2\pi h T_f l_{ki}}{6}\begin{bmatrix} 2R_i + R_k \\ 0 \\ R_i + 2R_k \end{bmatrix} \quad (32)$$

The capacitance matrix which is the unsteady state factor is given by the fourth Term of Eq. 12 and the sixth Term of Eq. 16, the transient Equation; it is derived as follows;

$$2\pi \iint_A [S]^T \left\{ \rho\, c\, \bar{r}\, \frac{\partial T}{\partial t} \right\} drdz$$

with

$$= \frac{\partial}{\partial t}\left(\begin{bmatrix} S_i & S_j & S_k \end{bmatrix} \begin{Bmatrix} T_i \\ T_j \\ T_k \end{Bmatrix} \right)$$

Thus

$$[C]^{(e)} = 2\pi\rho c \int_A \begin{bmatrix} S_i^2 & S_i S_j & S_i S_k \\ S_i S_j & S_j^2 & S_j S_k \\ S_i S_k & S_j S_k & S_k^2 \end{bmatrix} \begin{Bmatrix} \dot{T} \\ \dot{T} \\ \dot{T} \end{Bmatrix} \bar{r}\, drdz$$

Applying the Papus Guldinus theorem and simplifying,

We get;

$$[K]^{(G)}\{T(t)\}^{(G)} + [C]^{(G)}\left\{\frac{T(t) - T(t-\Delta t)}{\Delta t}\right\}^{(G)} = \{F(t)\}^{(G)} \quad (33)$$

Formation element Matrices to Global Matrix

$$[K]^{(G)}\{T(t)\}^{(G)} + [C]^{(G)}\left\{\frac{T(t) - T(t-\Delta t)}{\Delta t}\right\}^{(G)} = \{F(t)\}^{(G)}$$

For all the elements in the domain, assemble the global, conductance, capacitance, and thermal load matrices as well as the global matrix of the unknown temperature i.e. the element's conductance, capacitance and thermal load matrices have been obtained. All finite element analyses need the construction of these elements. The global matrix will be assembled to form the assemblage conductance, capacitance and thermal load matrixes.

Combining these components produces the subsequent finite element equation:

In general:

$$[K]^{(G)}\{T\}^{(G)} + [C]^{(G)}\{\dot{T}\}^{(G)} = \{F\}^{(G)} \quad (34)$$

$[k]^{(G)} = [k_c]^{(G)} + [k_h]^{(G)}$ = The global matrix of conductance caused by conduction and if there is a possible convection at the elementedge (s),

$\{T\}^{(G)}$ = Unknown temperature at each node at any time,

$[C]^{(G)}$= Capacitance global matrix caused by the transient equation,

$\left\{\dot{T}\right\}^{(G)}$ = Rate of change of temperature with respect to time,

$\{F\}^{(G)} = \{F_h\}^{(G)} + \{F_q\}^{(G)}$ = Global thermal load matrix if there is a possible convection at the

element edge (s), or if thereisheat generation respectively, in our case $\{F_q\}^{(G)} = 0$

The Euler approach

We shall be able to determine the nodal temperatures as a function of the time utilizing two-point recurrence formulae. In this work, Euler's approach, also known as the backward difference schemes (BDS), will be used to calculate the rate of change of temperature, as well as the temperature history at every point (node) on a steel bar. [35-41].

Once the derivative of temperature T with respect to time t is expressed in the backward direction and the step time is not equal zero, we get tha $(\Delta t \neq 0)$

$$\left\{[K]^{(G)}\right\}\{T(t)\}^{(G)} + [C]^{(G)}\left\{\frac{T(t)-T(t-\Delta t)}{\Delta t}\right\}^{(G)} = \left\{F(t)\right\}^{(G)} \quad (35)$$

where:

$\dot{T}$ = rate of temperature (°C/s);

T (t) = temperature of *t*s, (°C);

T (t - Δt)= temperature of (t - Δt) s, (°C)

Δt = step time chosen (s) and t = time (s) at starting time (t = 0)).

By modifying the values of temperature rate {T) in the global equation of the finite element, we obtain that;

$$[K]^{(G)}\{T(t)\}^{(G)} + [C]^{(G)}\left\{\frac{T(t)-T(t-\Delta t)}{\Delta t}\right\}^{(G)} = \{F(t)\}^{(G)} \quad (36)$$

Finally, the matrices become;

$$\left[[K]^{(G)}\Delta t + [C]^{(G)}\right]\{T\}_{i+1}^{(G)} = [C]^{(G)}\{T\}_i^{(G)} + \{F\}_{i+1}^{(G)}\Delta t \quad (37)$$

All of the right hand side of Eq. 37 is fully known at time t, including the initial condition at time t =0.

As a result, the temperature at each node for a subsequent time could be estimated given the temperature for the previous time.

Once a temperature history is given, the main mechanical characteristics of the bar of steel, such as hardness and strength, may be estimated.

3. APPLICATIONS

Estimation the history of temperature

The presented mathematical model has been applied to compute distribution of temperature with time in thermal analysis-transient of quenched steel specimen. Cylindrical shape of steel sample has been heated to 1000°C. After that, quenched in water to 32°C as ambient temperature, with water film coefficient of 5000 W/m^2·°C. History of temperature at each point of cylindrical steel specimen after quenched is being represented on Figures 7. & 8. The cylindrical specimen made from low carbon steels, with properties as mentioned below.

Thermal capacity, ρc (J/m^3·°C)

$$0 \le T \le 650\ ^\circ C,\quad \rho c = (0.004T + 3.3)\times 10^6$$

$$650 < T \le 725\ ^\circ C,\quad \rho c = (0.068T - 38.3)\times 10^6$$

$$725 < T \le 800\ ^\circ C,\quad \rho c = (-0.086T + 73.55)\times 10^6$$

$$T > 800\ ^\circ C,\quad \rho c = 4.55\times 10^6$$

Thermal conductivity, k (W/m·°C)

$$0 \le T \le 900\ ^\circ C,\quad k = -0.022T + 48$$

$$T > 900\ ^\circ C,\quad k = 28.2$$

In our study Eq. 34 becomes;

$$[K]^{(G)}\{T\}^{(G)} + [C]^{(G)}\{\dot{T}\}^{(G)} = \{F\}^{(G)}$$

And their respective equation;

$$[K]^{(G)} = [K_c]^{(1)} + [K_c]^{(2)} + [K_c]^{(3)} + [K_h]^{(1)} + [K_h]^{(3)} \quad (38)$$

$$[C]^{(G)} = [C]^{(1)} + [C]^{(2)} + [C]^{(3)} \quad (39)$$

$$\{F\}^{(G)} = \{F_h\}^{(1)} + \{F_h\}^{(3)} \quad (40)$$

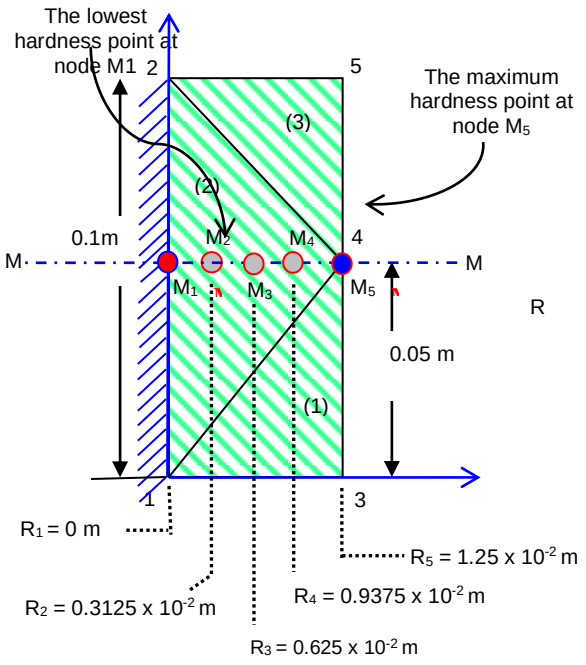

Figure 7. MM cross section of the domain

Slika 7. MM presek domena

A mathematical model is used to attain distribution of temperature at any point of quenched steel using boundary conditions and data inputs, for instance, is the transient-state temperature distribution estimates of five nodes from the center (M_1) to the surface (M_5) of quenched specimen which were calculated as illustrated on Figure 7 & Figure 8.

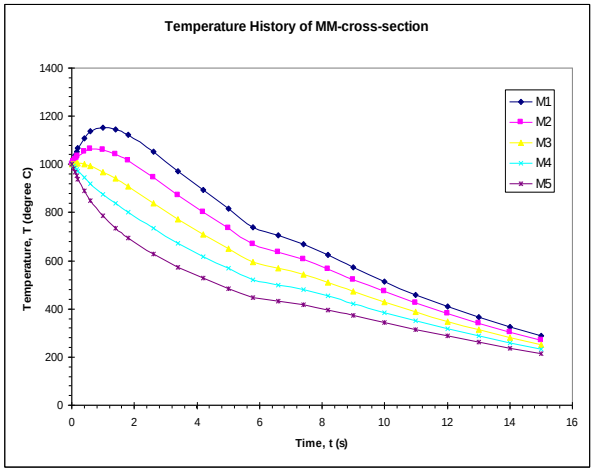

Figure 8. Temperature history of MM cross-section((0 ≤ R ≤0.0125 m), Z = 0.05 m).

Slika 8. Istorija temperature MM poprečnog preseka ((0 ≤ R ≤ 0,0125 m),Z = 0,05 m).

Verifying mathematical models

To validate temperature distribution results, the ANSYS program is utilised using the same input data of steel properties and boundary condition as in the mathematical model. Figurative representations of the temperature distribution from the ANSYS analysis are provided on Figs. 9.a & 9.b

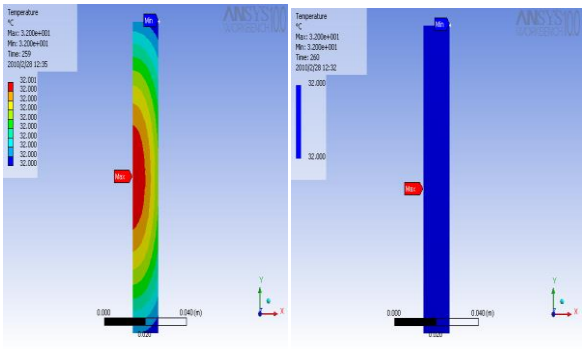

a *b*

Figure 9. a) distribution of temperature just before steel sample becomes entirely cooled and b)distribution of temperature at moment that entire steel specimen becomes completely cooled after 260s.

Slika 9. a) raspodela ᵗemperature neposredno pre nego što se čelični uzorak potpuno ohladi i b)raspodela temperature u trenutku kada se ceo čelični uzorak potpuno ohladi nakon 260s.

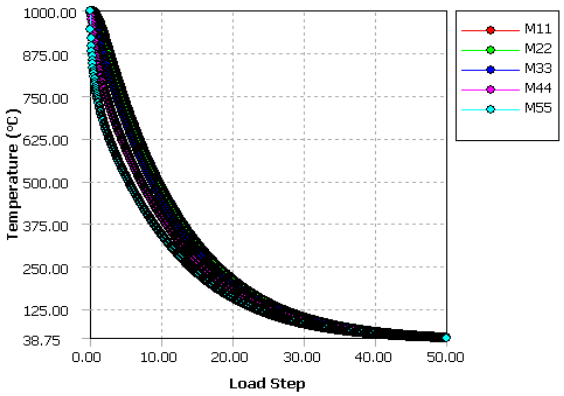

Figure 10. ANSYS-temperature vs time graph

Slika 10. ANSIS-temperatura u odnosu na vreme grafik

On Figure 10, temperature time graph from ANSYS analysis is presented;

The graphs on Figures 8 and 10 clearly demonstrate that the temperature history of quenched steel has the same patterns. Heat transfer is uniform throughout the steel specimen. Since the common cooling time, necessary for structural transformation for the majority of structural steels, is the time of cooling from 800 to 500°C (time $t_{8/5}$)[42-48]. So, there are two significant temperatures to consider when calculating the cooling time (800°C and 500°C). Then, essential mechanical properties including hardness may be calculated. According to the mathematical model for the 1st node with M_1 on the centre, quenching from 1000°C to 800°C takes 5.120 seconds, quenching from 1000°C to 500°C takes 10.442 seconds, while, time of cooling (t_c) takes 5.322 seconds.

Whereas by using ANSYS, we noticed that the quenching for the same node M_{11} were 3.932 seconds for 1000°C to 800°C and 9.618 seconds for 1000°C to 500°C, then time of cooling equal to 5.686 seconds. And it was reported that, for the mathematical model and ANSYS, t_c = 3.7944 and 4.762 sec respectively, for the nodes on the surfaces M_5 and M_{55}. It is clear from the aforementioned that both approaches strongly agreed.

Calculation LHP

Estimating the desired time of cooling

To compute the time of cooling, t_c, time for the (points) to cool from 850ºC to 800ºC is documented and subtracted by the time for the sample to cool until 500ºC.

$$t_c = t_{800} - t_{500}$$

We can calculate the time it took for node M_1 to reach 800ºC from Figure 3.

t_{800^oC} = 5.120s

Similarly, it takes 10.442 seconds for node M_1 to reach 500°C (t_{500^oC} = 10.442s).

Thus, the Node M_1 Cooling Time t_c;

$t_c = t_{500^oC} - t_{800^oC} = 10.442-5.120=5.322s$

The cooling time t_c was estimated in the same manner for nodes M_2 to M_5, with the final findings displayed in Table 1.

Table 1. Illustrates time of cooling t_c and cooling rate (ROC)

Tabela 1. Ilustruje vreme hlađenja tc i brzinu hlađenja (ROC)

Node	t_c (s)	ROC (°C /s)
M_1	5.322	56.368
M_2	5.218	57.494
M_3	5.082	59.028
M_4	4.790	62.636
M_5	3.794	79.064

Using the Standard Jominy distance vscooling time curve to get the Jominy distance

To acquire the appropriate Jominy distance, cooling time, t_c will now be fitted into the Jominy distance versus cooling time curve. Jominy distance may also be estimated via Microsoft Excel using polynomial expressions with polynomial regression.

The common Table [Cooling rate at each Jominy distance (Chandler, H., 1998)] will be utilised in this paper.

Therefore, using the data [from Cooling rate at each Jominy distance (Chandler, H., 1998)], the Jominy distance of nodes M_1 to M_5 will be determined. The final findings are provided in Table 2, where.

The definition of ROC, (Rate of Cooling);

$$ROC = \frac{800°C\text{-}500°C}{t_c} = \frac{800°C\text{-}500°C}{t_{500°C} - t_{800°C}} \ (°C/s)$$

Table 2. Time of cooling, Rate of cooling and Jominy distance of nodes M_1 to M_5

Tabela 2. Vreme hlađenja, Brzina hlađenja i Jomini rastojanje čvorova M1 do M5

Nodes	t_c (s)	ROC (°C /s)	Jominy distance (mm)
M_1	5.3222	56.368	7.0329
M_2	5.2179	57.494	6.9429
M_3	5.0823	59.028	6.8238
M_4	4.7896	62.636	6.5579
M_5	3.7944	79.064	5.5578

Estimate the hardness of a quenched steel specimen.

The HRC could be estimated using the Practical date Handbook, the Timken Company 1835 Duebex Avenue SW Canton, Ohio 44706-2798 1-800-223, www.timken.com, which demonstrated the relationship for this type of steel between J-Distance with HRC, and then HRC can be evaluated as previously explained. The final findings represented on Figure 11 &Table 3.

Table 3. Time of cooling, Rate of cooling, Jominy distance and HRC of nodes M_1-M_5, water-cooled by MM

Tabela 3. Vreme hlađenja, Brzina hlađenja, Jomini rastojanje i HRC čvorova M1 - M5, vodeno hlađeni MM

Nodes	t_c (s)	ROC (°C /s)	Jominy-distance (mm)	Hardness (HRC)
M_1	5.3222	56.368	7.0329	25.485
M_2	5.2179	57.494	6.9429	25.821
M_3	5.0823	59.028	6.8238	26.274
M_4	4.7896	62.636	6.5579	27.313
M_5	3.7944	79.064	5.5578	31.346

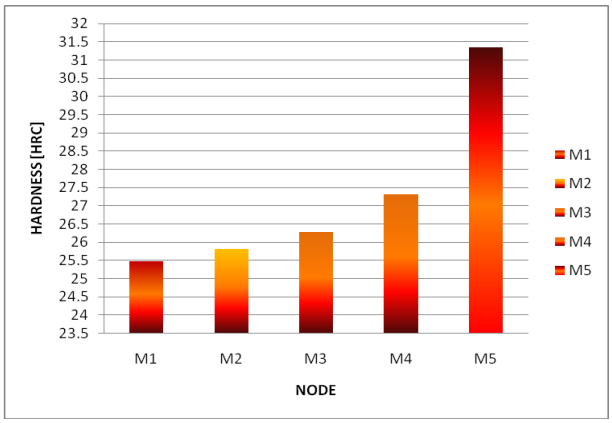

Figure 11. Distribution of hardness along the MM cross section at Z = 0.05m for nodes M_1 to M_5 from the centre to surface by developed mathematical model

Slika 11. Raspodela tvrdoće duž MM poprečnog preseka na Z = 0,05m za čvorove M1 do M5 od centra do površine razvijenim matematičkim modelom

Verification of mathematical models

The same procedure and steps taken to determine the hardness at each point even LHP of the quenched industrial steel bars by developed mathematical model as explained above, will be applied here by using ANSYS SOFTWARE analysis, from temperature-time graph by the ANSYS analysis which seen on Fig. 10, time of

cooling, rate of cooling, Jominy distance then LHP can be determined, the final results illustrated on Table 4 and Figure 12.

Table 4. Time of cooling, Jominy distance and HRC for nodes M_{11} to M_{55}, water cooled using ANSYS

Tabela 4. Vreme hlađenja, Jomini udaljenost i HRC za čvorove M11 do M55, vodeno hlađenje pomoću ANSIS-a

Nodes	Cooling time,	J-distance (mm)	HRC
M_{11}	5.696	7.352	24.34
M_{22}	5.689	7.340	24.37
M_{33}	5.686	7.327	24.42
M_{44}	5.525	6.937	25.83
M_{55}	4.762	6.53	27.4

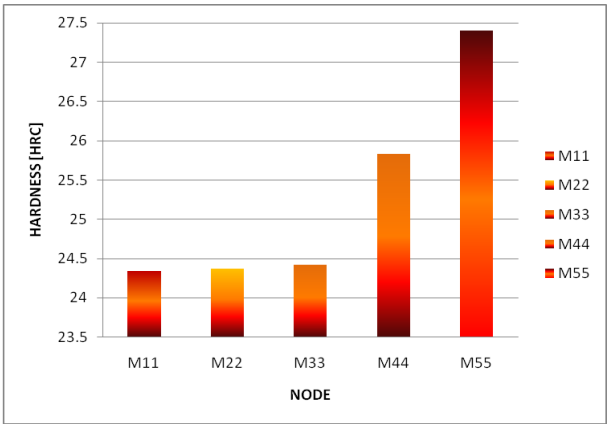

Figure 12. According to ANSYS, the distribution of hardness along the MM cross section at Z = 0.05m for nodes M_1 to M_5 from the centre to surface

Slika 12. Prema ANSIS-u, raspodela tvrdoće duž MM poprečnog preseka na Z = 0,05m za čvorove M1 do M5 od centra do površine

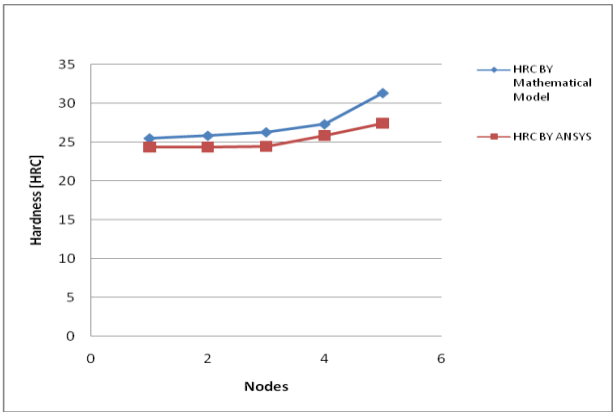

Fig. 13. The HRC comparison between the MM results and ANSYS

Slika 13. HRC poređenje između MM rezultata i ANSIS-a

Hardness comparison

The comparison of HRC between the mathematical model results for the nodes M_1-M_5 and ANSYS SOFTWARE results for the nodes M_{11}-M_{55} for the same quenched steel specimen shown below on Figure 13.

4. CONCLUSIONS

A steel quenching mathematical model has been constructed to determine the distribution of temperature thus cooling times, cooling rate, Jominy distance, and lastly the hardness of the quenched industrial steel bar at any position (point) even LHP in a cylindrical shape specimen. The finite element Galerkin residual approach is used to build the model. The numerical simulation of quenching consisted of numerical simulation of temperature transient field of cooling process. By comparing hardness findings with ANSYS software simulations, this mathematical model was examined and validated. According to the mathematical model and ANSYS findings, the nodes on the surface [M_5 and M_{55}] cool quicker than the nodes at half the length at the centre [M_1 and M_{11}] because $t_{Cm5} < t_{Cm1}$ and $t_{Cm55} < t_{Cm11}$, This means that the mechanical properties, such as hardness, will differ, with the hardness on the surface nodes [M_5 and M_{55}] being greater than the hardness on the centre nodes [M_1 and M_5] and this is which we found in our results by developed mathematical model as illustrated on Table 3, Fig. 11 and also by ANSYS Table 4, Figure12, where the hardness on the surface at the nodes [M_5 and M_{55}] equals 31.3 and 27.4 respectively, whereas the hardness at mid the length in the centre [M_1 and M_5] equals 25.485 and 24.34 respectively.

The results indicated that the node at the surface, such as M_5 and M_{55}, will be the 1st to completely cool after quenching because it is in contact with the cooling medium, followed by the other nodes on the radial axis to the centre, respectively. The final point will completely cool after quenching will be at mid the length in the centre, like in our study with M_1 and M_{11}. As a result, LHP will be half the length of the quenched industrial steel bar at its centre. It will be more necessary to understand LHP once the radius of the quenched steel specimen is high because LHP will be low, that is, lower than the hardness on the surface, implying that increasing the radius of the bar is inversely proportional to LHP.

It is clear that the developed mathematical model has been verified and validated by comparing its temperature simulation and hardness findings withcommercial finite element program,

ANSYS simulations. The comparison shows that the proposed model is reliable.

Acknowledgement

The authors gratefully acknowledge the Bright Star University, El-Brega - Libya and University of Tobruk, Libya for supporting this Manuscript.

5. REFERENCE

[1] R.G.Rahel, A.S.Elmaryami, M.A.Ahmida, A.A.Haj (2022) Computer Simulation to Determine LHP of 4 Different Types of Transient Industrial Quenched Molybdenum Steel Bars. European Journal of Engineering and Technology Research. 7(6), 51–55. https://doi.org/10.24018/ejeng.2022.7.6.2873.

[2] X.Bing, G.Xiao-Wei, J.Wei-Wu, C.Miao, L.Jun (2022) Galerkin free element method and its application in Fracture Mechanics, Engineering Fracture Mechanics, 218, 106575.

[3] A.S.Elmaryami, B.Omar (2012) Developing 1-dimensional transient heat transfer axi-symmetric MM to predict the hardness, determination LHP and to study the effect of radius on E-LHP of industrial quenched steel bar. Heat Transfer Phenomena and Applications, p.153-182.

[4] G.Oguntala, G.Sobamowo (2016) Galerkin's Method of Weighted Residual for a Convective Straight Fin with Temperature-Dependent Conductivity and Internal Heat Generation. International Journal of Engineering and Technology (IJET), 6(12), 432-442.

[5] A.S.Elmaryami (2021) Unsteady state computer simulation of 2 chromium steel at 925°C as austenitizing temperature to determine the lowest hardness point (LHP). Journal of Metallurgical & Materials Engineering, 18(2), 79-91.

[6] G.M.Sobamowo, A.A.Yinusa, Z.O.Dere, R.O. Saheed, R.O.O.Gbadamosi (2022) Unsteady state heat transfer analysis of a convective-radiative rectangular fin using Laplace Transform-Galerkin weighted residual method, Journal of Engineering and Thermal Sciences, 2(2), 84–99, https://doi.org/10.21595/jets.2022.22807

[7] A.S.Elmaryami, B.Omar (2012) Developing1D MM of axisymmetric transient quenched chromium steel to determine LHP. Journal of Metallurgy, 9, ID 539823.

[8] M.M.Khader, M.M.Babatin, Ah.M.Megahed, A.Eid (2022) Implementing the Galerkin Method Associated with the Shifted Vieta-Lucas Polynomials for Studying Numerically the Bionanofluid Flow Which Is Saturated by Gyrotactic Microorganisms over a Slippery Stretching Sheet,Journal of Mathematics, 2022, ID 5236196, https:// doi.org/10.1155/2022/5236196

[9] R.K.Quenching (2001) Tempering of Welded Steel Tubular.[Internet] Retrieved from:https://www. thefabricator.com/thefabricator/article/tubepipefabricati n/quenching-and-tempering-of-welded-carbon-steel-tubulars.

[10] L.Sadek, A.S.Bataineh, H.T.Alaoui, I.Hashim (2023) The Novel Mittag-Leffler–Galerkin Method: Application to a Riccati Differential Equation of Fractional Order. Fractal and Fractional, 7(4),302-311. https://doi.org/10.3390/fractalfract7040302

[11] H.Cheng, Z.Xing, Y.Liu (2023) The Improved Element-Free Galerkin Method for 3D Steady Convection-Diffusion-Reaction Problems with Variable Coefficients. Mathematics, 11, ID 770. https:// doi.org/10.3390/math11030770

[12] A. Ab Aziz et al. 2019) Comparative Study of Collocation Method and Galerkin Method for Solving Nonlinear Partial Differential Equation, International Journal of Advanced Trends in Computer Science and Engineering, 8(1.5), 1 – 4.

[13] S.M.Afzal Hoq, E.Sulaeman, A.Okhunov (2016) Error Analysis of Heat Conduction Partial Differential Equations using Galerkin's Finite Element Method, Indian Journal of Science and Technology, 9(36), 1-6, 10.17485/ijst/2016/v9i36/ 102158,

[14] S.Ġ.Araz, H.D.Galerkin (2018)Method for Numerical Solution of Two Dimensional Hyperbolic Boundary Value Problem with Dirichlet Conditions, Araz&Durur/Kırklareli University Journal of Engineering and Science, 4(1), 1-11.

[15] H.K.Ching, S.C.Yen (2005) Meshless local Petrov-Galerkin analysis for 2D functionally graded elastic solids under mechanical and thermal loads, Composites Part B: Engineering, 36(3), 223-240.

[16] Y.Li, J.Li, P.H.Wen (2019) Finite and infinite block Petrov–Galerkin method for cracks in functionally graded materials, Applied Mathematical Modelling, 68, 306-326

[17] Ch.Heng, M.Peng (2022) The Improved Element-Free Galerkin Method for 3D Helmholtz Equations. Mathematics, 10(1), 14-22.

[18] A.Elmaryami, H.M.Khalid, A.Alamaria, O.Alashebe, S.Ali, A.Salem, R.Khaled (2021) Determination the Corrosion Rate of Carbon Steel (0.4%C) Due to Thermal Cycling, Oil Cooled. Tecnica Italiana-Italian Journal of Engineering Science, 65(1), 74–78.https://doi.org/10.18280/ti-ijes.650111.

[19] A.Elmaryami, H.M.Khalid, A.M.Abdulssalam, A.A.Abdulssalam, M.M.Alssafi, A.S.Abdullateef, Z.A.Mohamed (2021) Design of a Simple Model of S. P. P. to Study the Effect of Increasing the Boiler Pressure on the Efficiency of the Model. Engineering &Amp; Technology Review. 2(1), 1–7. https://doi.org/10.47285/etr.v2i1.60.

[20] A.S.Elmaryami, B.Omar (2020) A Novel (1-D) Mathematical Modeling toDetermine (E-LHP) of Industrial Transient Heat Transfer QuenchedChromium Steel 5147H, Sea Water Cooled. Tecnica Italiana-ItalianJournal of Engineering Science. 64(2-4), 251-258.

[21] K.G.Budinski (1992) Engineering Material: Properties and Selection. 4th ed.Prentice Hall International. p.285-309.

[22] A.S.Elmaryami, A.S.Salem, S.S.Ali, H.O.Mokhtar, R.A.Khaled (2020) Corrosion rate calculation of carbon steel (0.4% C) after subjected tothermal cycling, sea water cooled. Journal of Multidisci-plinaryEngineering Science and Technology, 1(1), 28-34.

[23] S.Moaveni (2011) Finite element analysis theory and application with ANSYS, 3/e. Pearson Education India.

[24] A.S.Elmaryami, Ab.Sousi, W.Saleh, Sh.El-Mabrouk, Ab.El-Mawla, M.Elshayb (2019) Maximum Allowable ThermalStresses Calculation of Water Tube Boiler during Operation.International Journal of Research-Granthaalayah, 7(7), 191-199.

[25] A.S.Elmaryami, B.Omar (2011) Developing 1-D mm of axisymmetrictransient quenched molybdenum steel AISI-SAE 4037H to determinelowest hardness point. Journal of Metallurgy and Materials Science, 53(3), 289-303.

[26] J.Fuhrmann, D.Hömberg (1999) Numerical simulation of the surfacehardening of steel. International Journal of Numerical Methods forHeat & Fluid Flow., 9(6), 705-724.

[27] A.S.Elmaryami, B.Omar, F.A.Ali, S.A.Mohammad, A.K.Ahmad, B.E.Wael, A.A.Moftaah (2015) Study of LHP and Effect of Radius in Heat Treated steel 1045 Bar by 1-D FEM Modeling. International Journal of Engineering and Applied Sciences, 7(5), 50-58.

[28] A.S.Elmaryami, B.Omar (2013) Transient Computer Simulation of Industrial Quenched Steel Bar to Determine the Lowest Hardness Point of Molybdenum and Boron Steel at 850 C as Austenitizing Temperature Quenched in Different Medium. International Journal of Materials Science, 8(1), 13-28.

[29] H.Chandler (1999) Hardness testing. ASM international.

[30] A.S.Elmaryami, A.Alsoussi, M.Gomaa, E.Abd-Allah (2017) Determination the cooling time, rate of cooling, jominy distance andthe hardness during heat transfer of quenched steel bar. Journal ofScience-Garyounis University, 38(5), 1-11.

[31] A.S.Elmaryami, B.Omar (2013) Modeling the effect of radius on temperaturehistory of transient quenched boron steel. Acta Metallurgica Slovaca,19(2), 105-111.

[32] S.Moaveni(2003) Finite Element Analysis. A Brief History of the FiniteElement Method and ANSYS. 6-8, Pearson Education, Inc.

[33] A.S.Elmaryami, B.Omar (2013) Effect of radius on temperature history oftransient industrial quenched chromium Steel-8650H by developing 1- D MM. Applied Mathematical Sciences, 7(10), 471-486.

[34] R.Rahel, A.S.A.Elmaryami, M.A.Ahmid, A.A.Ahmed (2022) Computer simulation to determine LHP of 4 different types of transient industrial quenched molybdenum steel Bars, European Journal of Engineering and Technology Research, 7(6), 51-55.

[35] S.A.Abdlmanam, A.Elmaryami, M.Elshayeb, B.Omar, P.Basu, S.B.Hasan (2013) Development of a numerical model of quenching of steel bars for determining cooling curves. Metal Science and Heat Treatment, 55(3), 216-219.

[36] B.Omar, A.S.Elmaryami (2013) Developing 1-D MM of transient industrialquenched chromium steel-5147H to study the effect of radius ontemperature history. Advanced Materials Research. 711, 115-127.

[37] A.S.Elmaryami (2007) Effect of Thermal Cycling on the Corrosion andMicrostructure of Plain Carbon Steels. Materials science & technology conference and exhibition: MS&T'07. 6, 3771-3784.

[38] A.S.Elmaryami, B.Omar (2012) Modeling LHP in carbon steel-1045 during quenching. Journal of Mathematical Theory and Modeling, 2(12), 35-47.

[39] A.S.Elmaryami, B.Omar (2012) Determination LHP of axisymmetric transient Molybdenum steel-4037H quenched in seawater by developing 1-d mathematical model. Metallurgical and Materials Engineering, 18(3), 203-222.

[40] A.S.Elmaryami, B.Omar (2012) Modeling the lowest hardness point in a steel bar during quenching. Materials Performance and Characterization, 1(1), 1-15.

[41] M.A.Ahmida, A.S.Elmaryami (2022) Investigation of Using Physical Optical Reflectivity Probes in Evaluating and Monitoring Powder Mixtures of Sugar and Slag. Instrumentation Mesures, Métrologies, 21(2), 43-48.

[42] A.S.Elmaryami, B.Omar (2011) The lowest hardness point calculation bytransient computer simulation of industrial steel bar quenched in oil atdifferent austenitizing temperatures. in 2011 International Conferenceon Management and Service Science. 1, 1-6. doi.10.1109/ICMSS. 2011.5999335

[43] S.A.Abdlmanam, A.Elmaryami, S.B.Hasan, B.Omar, M. Elsayebl (2009) Unsteady state hardness prediction of industrial quenched steel bar [one and two dimensional]". Materials Science and Technology Conference and Exhibition 2009, MS&T'09. Pittsburgh, PA; USA; 3, 1514-1520. Scopus.

[44] A.S.Elmaryami (2008) Effect of thermal cycling on hardness of plain carbonsteels. Materials Science and Technology Conference and Exhibition, MS&T'08. Pittsburgh, PA; United States. 1(3), 1502-1514.

[45] A.S.Elmaryami, B.Omar (2011) Effect of Austenitizing Temperatures onHardness of Two Chromium Steel Quenched in Sea Water by Unsteady State Computer Simulation. Materials Science & Technology[MS&T'11] Conference & Exhibition; Columbus, Ohio,USA.

[46] B.Omar, M.Elshayeb, A.S.Elmaryami (2009) The Microstructures andCorrosion of Carbon Steel after Subjected to Heat Treatment thenThermal Cycling, Water Cooled. 5th European Metallurgical Conference. 1(4), 1492- 1495.

[47] S.A.Abdlmanam, S.B.Hasan, O.Badrul, M.Elsahbi (2009) Unsteady state thermal behavior of industrial quenched steel bar". 18 th World IMACS Congress and International Congress on Modelling and Simulation: Interfacing Modelling and Simulation with Mathematical and Computational Sciences, MODSIM09; Cairns, QLD; Australia; p. 1699-1705.

[48] A.S.Elmaryami, B.Omar (2011) Projjal Basu and Suleman Bin Haji Hasan "Unsteady State Computer Simulation of 2 Chromium Steel at 850°C as Austenitizing Temperature Quenched in Different Medium". Proceedings of the ASME 2011 International Manufacturing Science and Engineering Conference, MSEC2011, Corvallis, Oregon, USA.

IZVOD

NOVO 2-D MATEMATIČKO MODELIRANJE ZA ODREĐIVANJE LHP ZA ZAŠTITU INDUSTRIJSKOG PROLAZNOG TOPLOTNOG TRETMANA KALJENI NISKOUGLJENIČNI ČELICI BAR

2-dimenzionalni matematički model osovine simetrične tranzijentne industrijske šipke od niskougljeničnog čelika, da bi se ispitao uticaj istorije procesa na metalurške i karakteristike materijala, usvojen je vodeno hlađeni model zasnovan na tehnici konačnih elemenata. Dvodimenzionalni osnosimetrični matematički model je korišćen za predviđanje istorije temperature i, kao rezultat, tvrdoće kaljene čelične šipke u bilo kom čvoru (tački).Ocenjuje se LHP (najniža tačka tvrdoće). U ovom radu, tvrdoća tačaka uzorka je procenjena transformacijom utvrđenog karakterističnog vremena hlađenja za faznu konverziju t8/5 u tvrdoću. Model se može koristiti kao smernica za dizajniranje pristupa hlađenju da bi se postigla željena mikrostruktura i mehanička svojstva, na primer, tvrdoća. Matematički model je verifikovan i validiran upoređivanjem njegovih rezultata tvrdoće sa rezultatima komercijalnog softvera konačnih elemenata. Poređenje pokazuje da je predloženi model pouzdan.

***Ključne reči**: toplotna obrada, gašenje, ososimetrična čelična šipka, konačni elementi, 2-D matematičko modeliranje, prenos toplote u nestabilnom stanju.*

Naučni rad
Rad primljen: 20.03.2023.
Rad korigovan: 11.05.2023.
Rad prihvaćen: 15.05.2023.
Rad je dostupan na sajtu:www.idk.org.rs/casopis